OCTOBER 01 2008

On sound propagation from a slanted side branch into an infinitely long rectangular duct

S. K. Tang; G. C. Y. Lam

J. Acoust. Soc. Am. 124, 1921–1929 (2008)
https://doi.org/10.1121/1.2968671

On sound propagation from a slanted side branch into an infinitely long rectangular duct

S. K. Tang[a] and G. C. Y. Lam
Department of Building Services Engineering, The Hong Kong Polytechnic University, Hong Kong, China

(Received 6 September 2007; revised 4 March 2008; accepted 10 July 2008)

The transmission of sound from a slanted side branch into an infinitely long rectangular duct is studied numerically using the method of finite element with absorptive domain exit boundaries. The sound transmission coefficients associated with various acoustic modes are investigated in details. The results show that the plane wave assumption is only valid at very low frequency. It is also found that the intensities of the higher modes are stronger than that of the plane wave once they are excited. Besides, a critical side-branch slant angle is found over which a significant change of sound propagation mode takes place. This affects substantially the energy distribution between various acoustic modes inside the main duct. A simplified model is proposed to explain the phenomenon and the relationship of this critical angle with the width ratio between the side branch and the main duct is established. © *2008 Acoustical Society of America.* [DOI: 10.1121/1.2968671]

PACS number(s): 43.20.Mv [LT] Pages: 1921–1929

I. INTRODUCTION

Complicated duct works are very common in modernized air-conditioned buildings. Their primary functions are to convey the treated air with the right temperature and humidity into the occupied zones and to provide a controlled route for the extraction of the used air out of the same areas. However, noise from the ventilation systems will propagate along these duct works and thus affect the indoor acoustical environment.[1]

Duct junctions are very frequently found in the ventilation ducting network. Usually, they are found at locations where a smaller duct merged into a main duct or where a main air duct forks into smaller ducts. The noise propagation between these ducts depends on the junction configuration. Conventionally, duct junctions are right angled and the noise transmission across these junctions has attracted the attention of many researchers for improved prediction and duct noise control. Typical examples include the works of Miles,[2] Bruggeman,[3] Redmore and Mulholland,[4] Dubos *et al.*,[5] and more recently Tang.[6] Effects of coupled side branches on sound transmission along a main duct were examined experimentally by Tang and Li.[7] There are also related studies such as that of Davies[8] for connected corridors with rectangular cross sections, that of Lippert[9] for right-angled duct bends, and those related to waveguides (for instance, Razavy[10] and Lee *et al.*[11]). However, many of these studies are restricted in the low frequency range because the waves involved can be analytically handled and the plane waves can be measured readily using the conventional transfer function method.[12]

In a heavily serviced building, many services are located in the very congested ceiling voids and very often the right-angle junction configuration does result in additional constraints in the space utilization. Also, such junction will also be accompanied with flow bends, resulting in high static pressure losses in the duct work. A slanted junction appears to be able to help reduce the spatial constraint and to some extent smoothing the flows around the junctions, resulting in smaller pressure loss and weaker turbulence intensity, which in turn has an impact on the aeroacoustic radiation (for instance, Dequand *et al.*[13]). Slanted junctions may also help reduce the amount of material used.

The present study is an attempt to understand how sound propagates from a long slanted side branch into an infinitely long duct in the absence of a flow. The cross section of the duct and side branch are taken to be rectangular as rectangular ducts are the most commonly found duct type in commercial buildings with centralized air-conditioning and ventilation systems. The duct and the side branch are of the same spanwise length (very common case as well) such that no excitation in the spanwise direction is possible. The present adopted system is exactly a two-dimensional one. The interactions between the various duct modes are examined. The finite element method adopted in the recent studies of S.K.T. is used.[6,14] It is hoped that the present results can provide information for improved acoustical design of the air-conditioning and ventilation duct work. The present study also forms part of a comprehensive investigation on the sound propagation across duct junctions with and without flows.

II. THE COMPUTATIONAL DOMAINS

Figure 1 shows the junction configuration and the nomenclature adopted in the present study. In practice, the side branches are not wider than the main duct and thus $b \leqslant a$. One should note that the interfacial length between the slanted side branch and the main duct varies with b and the slant angle θ. In the present study, a plane wave is set to propagate toward the junction from the slanted side branch.

The finite element computational approach of Tang and Lau[14] and Lau and Tang[15] is adopted in the present study. The wave equation to be solved is the Helmholtz equation:

[a]Author to whom correspondence should be addressed. Electronic mail: besktang@polyu.edu.hk

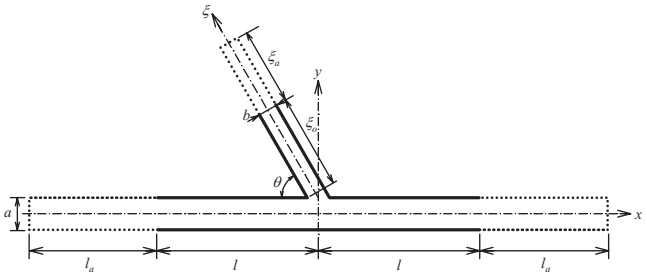

FIG. 1. Schematic of the slanted side-branch junction and nomenclature. (Dotted lines represent locations of absorptive boundaries.)

$$\nabla^2 p + k^2 p = q, \tag{1}$$

where q is the source, p is the acoustic pressure, and k the sound wave number. For the low frequency range where the frequency of sound is below the first eigenfrequency of the main duct, one can expect that only plane waves exist at locations far away from the junction. The boundary conditions can be analytically written as

$$\frac{\partial p}{\partial n} + ikp = \begin{cases} 2ik & \text{at } \xi = \xi_0 \\ 0 & \text{at } x = l \\ 0 & \text{at } x = -l, \end{cases} \tag{2}$$

where $i=\sqrt{-1}$, n represents the unit outward normal of a surface and $q=0$. The computational domain is bounded within $|x| \leqslant l$ and $0 \leqslant \xi \leqslant \xi_0$. Outgoing plane wave condition at $x=l$ and $x=-l$ are adopted, while the condition at $\xi=\xi_0$ represents a unit plane wave excitation together with a plane wave reflection in the positive ξ direction. For higher frequencies, higher modes exist and the plane wave excitation is, as depicted in Tang and Lau,[14]

$$q = 2ke^{i\gamma}\delta(\xi - \xi_0), \tag{3}$$

where δ is delta function and γ is an arbitrary phase angle of the excitation. The latter is not important in the present study and without loss of generality, it is set at $\pi/2$. The computation domain is extended to cover the regions with absorptive boundaries (dotted lines in Fig. 1) having

$$\frac{\partial p}{\partial n} + ik\alpha p = 0, \tag{4}$$

where α is an arbitrary absorption coefficient which varies with distance Δ from each interface between the normal domain and the absorptive domain. It vanishes at the location of the interface and increases very slowly in the beginning to ensure that no numerical reflection is produced at the interfaces. In the present study, $\alpha=0.01\Delta^2$.

The higher modes are completely damped within these regions before they reach the ends of the absorptive domains, where the outgoing plane wave conditions are again adopted. More details of these settings and their performance can be found in Tang and Lau[14] and Lau and Tang[15] and thus are not repeated here. In the present study, l is set at $20a$ and $\xi_0=20b$. The lengths of the absorptive regions are $30a$ for the main duct (l_a) and $30b$ for the slanted side branch (ξ_a).

The finite element computations are implemented using the software MATLAB[16] and the mesh generation is done through the Delaunay triangular algorithm.[17] Figure 2 illustrates an example of the meshes adopted in the higher frequency computations. For the meshes adopted in the present study, over 95% of the mesh triangles have a mesh quality index greater than the acceptable level of 0.6.[16] Also, the largest mesh has its length approximately 1/26 of the smallest wavelength involved in the present computation. It has been checked that any further refinement of the meshes will not produce noticeable variations in the results.

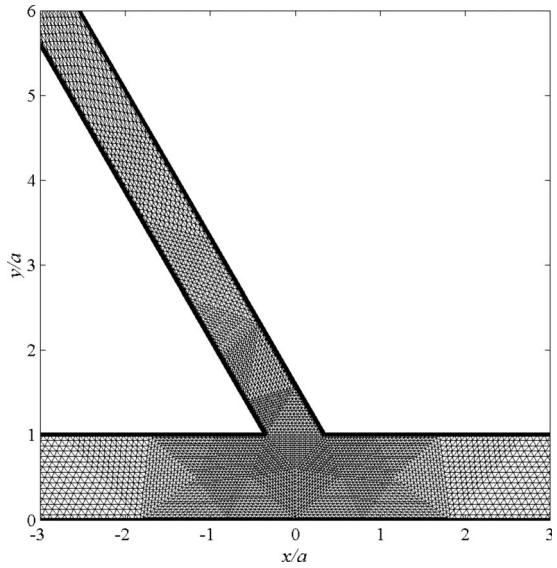

FIG. 2. Example of the finite element meshes adopted for $b/a=0.6$ and $\theta=60°$.

III. SOME THEORETICAL CONSIDERATIONS

In general, analytical solution for sound propagation across the slanted junction is very difficult if not impossible unless the sound frequency is very low. Peake[18] demonstrated the use of the Wiener–Hopf technique for the slanted nozzle exit, but an analytical solution is still not possible even at low frequencies.

When the wavelength of the sound is much larger than the physical dimension of the junction cross section, the acoustic pressure within a large region around the junction can be assumed to be uniform. Standard technique for plane wave calculation[19] suggests that the sound pressure magnitude in the main duct is, for a unit strength plane wave excitation in the slanted branch,

$$|p_d^+| = |p_d^-| = \frac{b}{a+0.5b} \Rightarrow \tau^+ = \tau^- = \frac{ab}{(a+0.5b)^2}, \tag{5}$$

where τ is sound power transmission coefficient, the suffix d denotes the quantity associated with the main duct, and the positive and negative prefixes denote downstream and upstream of the junction, respectively. The magnitude of the corresponding reflected wave in the side branch, $|p_r|$, is

$$|p_r| = \frac{2a-b}{2a+b}. \tag{6}$$

It should be noted that Eqs. (5) and (6) are independent of the slant angle θ at this low frequency situation.

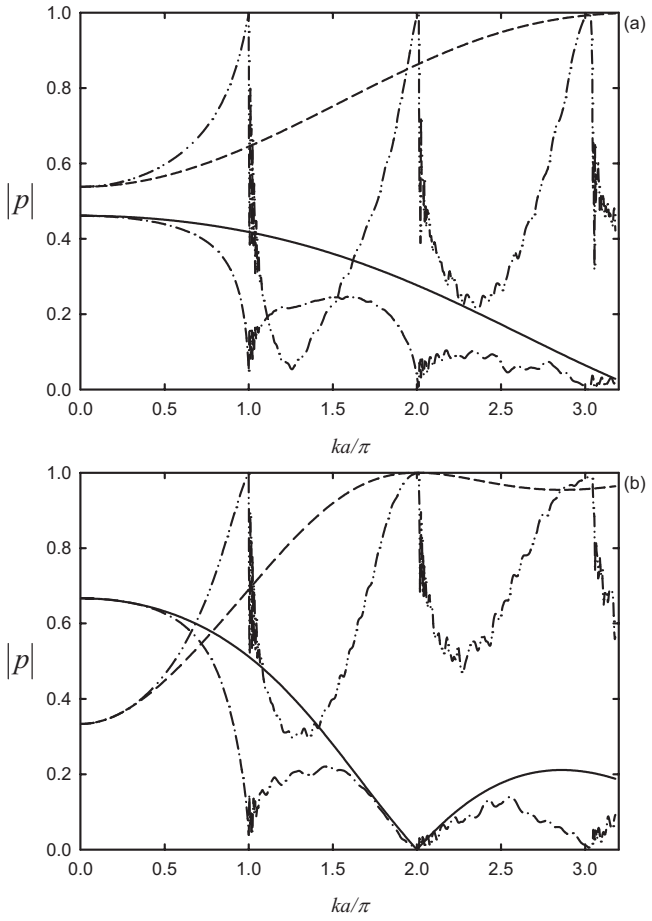

FIG. 3. Comparison between plane wave theory and numerical results for plane wave magnitudes for $\theta=90°$. (a) $b/a=0.6$ and (b) $b/a=1$. (—) In main duct from plane wave theory; (---) in side branch from plane wave theory; (–·–) in main duct from finite element computation; and (–···–) in side branch from finite element computation.

Numerical studies adopting the mode coupling technique or the finite element method have been done for $\theta=90°$ (for instance, Redmore and Mulholland[4] and Tang[6]). However, analytical solution for this slant angle is only possible when all the higher modes and the evanescent waves are ignored. Assuming the exit of the side branch acts as a massless piston exciting plane wave propagation inside the main duct, it is not difficult to show that for an unit strength plane wave excitation in the branch,

$$p = \frac{2\sin(kb/2)}{ka - i\left[1 - e^{-ikb/2}\dfrac{\sin(kb/2)}{kb/2}\right]} e^{-ik(|x|+\phi)}, \tag{7}$$

where ϕ is a constant related to the phase of the wave excitation inside the side branch and use has been made of the analytical formulas provided by Huang[20] for purely plane wave motion. Equation (7) converges to Eq. (5) when $ka \to 0$, and thus $kb \to 0$ as $a \geqslant b$. However, Eq. (7) overestimates the planar sound powers inside the main duct in the presence of higher modes or evanescent waves as shown in Fig. 3. The corresponding reflected wave is

$$p_r = \frac{1 - ika - e^{-ikb/2}\dfrac{\sin(kb/2)}{kb/2}}{1 + ika - e^{-ikb/2}\dfrac{\sin(kb/2)}{kb/2}} e^{-ik(y+\phi)}. \tag{8}$$

Again, Eq. (8) converges to Eq. (6) when $ka \to 0$. However, Eq. (8) does not model well the reflected wave in the side branch (Fig. 3). In conclusion, the plane wave assumption can only predict the wave magnitudes for $ka < 0.2\pi$ at $b/a=0.6$ [Fig. 3(a)] and for $ka < 0.4\pi$ at $b=a$ [Fig. 3(b)]. Though it seems that Eqs. (6) and (8) are able to give better predictions for $b=a$ than for $b=0.6a$, one should note that the controlling parameter in the plane wave assumption is b while the duct eigenfrequencies are more important in reality and they are related to a. One should also note that $\theta=90°$ is a very special case in the present study because asymmetric modes are not able to propagate inside the side branch under this right-angled junction situation.

IV. RESULTS AND DISCUSSIONS

In the foregoing discussions, the magnitudes of the plane waves and those of the higher modes inside the main duct are obtained at a distance $19a$ from the junction center (before any absorptive boundary) using the conventional orthogonal modal decomposition technique.[21] The corresponding location is $\xi=19b$ in the side branch. It should be noted that the magnitudes of the waves in the main duct and those of the reflected waves inside the side branch are independent of distance from the junction provided that the latter is larger than twice the duct/branch width.[22] It has been tested that the adopted long absorptive boundaries are able to eliminate backreflections into the computational region with rigid boundaries.

The magnitudes of the plane waves transmitted into the main duct and reflected back into the side branch are illustrated in Fig. 4. Those for $\theta=90°$, which have been shown in Fig. 3, are also presented here for the sake of easy comparison.

Concerning the plane wave propagating downstream of the junction in the main duct [Fig. 4(a)], the wave pressure magnitude (and thus the energy it carries) increases with decreasing θ when the sound frequency is low enough and then falls sharply at ka approaches π (the first main duct eigenfrequency). The larger the slant angle, the more rapid the fall of the wave magnitude. The wave magnitude also increases slightly as frequency increases for $\theta < 45°$ and $ka < \pi$, but the opposite is observed when $\theta \geqslant 52.5°$. The wave magnitude increases with the sound frequency for a relatively narrow ka region after $ka=\pi$ in general. For $\theta \leqslant 45°$, the variation of the wave magnitude with ka appears to be wavier and a local minimum is found at $ka \sim 1.57\pi$. The curves in Fig. 4(a), except that for $\theta=90°$, appear to converge at $ka=5\pi/3$, which corresponds to the first eigenfrequency of the side branch. It should be noted that there is no asymmetric mode propagation in the side branch for $\theta=90°$ as mentioned before.

The cut-on of the first asymmetric mode in the side branch also marks the beginning of a frequency region where

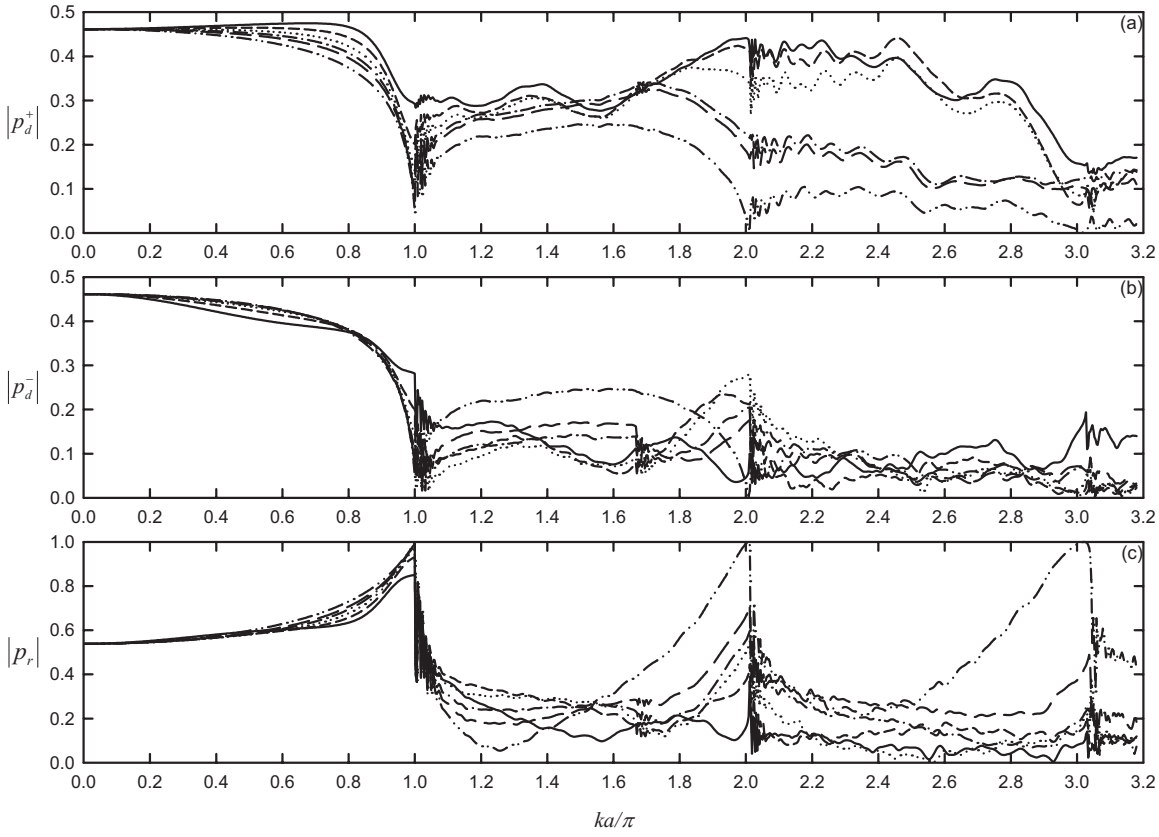

FIG. 4. Variations of plane wave magnitudes with frequency for $b/a=0.6$. (a) Downstream going wave in main duct; (b) upstream going wave in main duct; and (c) upstream going wave in the side branch. (—) $\theta=30°$; (---) $\theta=37.5°$; (···) $\theta=45°$; (–·–) $\theta=52.5°$; (——) $\theta=60°$; (–···–) $\theta=90°$.

the plane wave magnitude either continues to rise or starts to fall upon further increase of the sound frequency, and the transition between these two distinctive phenomena actually takes place within a very narrow range of θ [Fig. 4(a)]. For $b/a=0.6$, the transition takes place within $45° \leqslant \theta \leqslant 52.5°$ and the critical slant angle, θ_c, is expected to depend on b/a. This will be discussed and explained further later. A fall of the wave magnitude is again observed at $ka \sim 2\pi$, when the second eigenmode of the main duct is excited. It should be noticed that the plane wave magnitude after the excitation of the first eigenmode of the main duct for $45° < \theta < 60°$ is comparable to that at low frequency, but it does not mean that the acoustical energy contained in the higher modes will be insignificant within this slant angle range. Again, further discussions will be given later.

The plane wave propagating upstream of the junction carries less amount of acoustical energy than that propagating downstream for all slant angles studied as illustrated in Fig. 4(b). Before the first eigenfrequency of the main duct and for $ka < 0.8\pi$, the wave magnitude increases with increasing θ, because of the weaker diffraction round a more acute angle. This trend reverses at $ka > 0.8\pi$ followed by a rapid fall of the wave magnitude as $ka \rightarrow \pi$. The results in Fig. 4(b) are also indicating a change in the mode of wave propagation takes place within $45° \leqslant \theta \leqslant 52.5°$. One can notice that the cut-on of the first asymmetric higher mode in the side branch has a stronger effect on this upstream going plane wave than on the downstream going plane wave, especially for large slant angles (except $\theta=90°$).

At low frequency, the magnitude of the reflected wave increases with increasing slant angle and sound frequency as shown in Fig. 4(c). This is rather expected as stronger reflection back into the side branch takes place at larger slant angle. One can also notice from Fig. 4 that the acoustical energy carried by the plane wave is not high for $ka > 2\pi$. This energy is insignificant for small slant angles. The propagation of the higher modes will be discussed later.

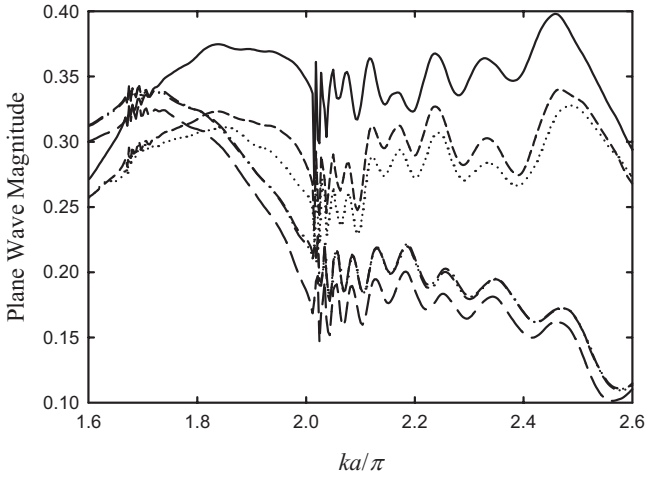

FIG. 5. Effects of slant angle on the downstream going plane wave magnitudes after the cut-on of the side-branch higher mode. (—) $\theta=45°$; (---) $\theta=49°$; (···) $\theta=52°$; (–·–) $\theta=52.5°$; (——) $\theta=53°$; (–···–) $\theta=60°$.

Figure 5 illustrates the plane wave magnitude in the main duct downstream of the junction for $45° < \theta < 60°$ and $1.6 < ka/\pi < 2.6$, which is the parameter range in which a change of the propagation mode of the plane wave is expected to occur. One can observe that the change takes place within a very narrow θ range at $\sim 52°$ to 52.5° and this change is abrupt. The results for $\theta = 53°$ almost overlap with those for $\theta = 52.5°$.

One can expect that a plane wave is more easily forced if there is a more uniform acoustical energy distribution at the region of the main duct just downstream of the junction. Plane wave passes through the slanted exit of the side branch, hits and reflected by the opposite main duct wall to set up the wave pattern at the junction. A very asymmetric pattern does not favor plane wave propagation and this happens when the slant angle is large as shown in Fig. 6(a) ($\theta = 90°$ and $ka = 1.8\pi$). At this condition, standing wave is setup inside the junction, making the acoustic pressure at the exit of the junction far from uniform. One should note that the acoustic pressure in the middle of the junction is out of phase with that at the opposite wall inside the junction in Fig. 6(a).

The corresponding acoustic pressure patterns for $\theta = 52.5°$ and 30° are given in Figs. 6(b) and 6(c), respectively. Though the acoustic pressures at the junction exit for these slant angles are still not uniform, that for $\theta = 30°$ appears to be more uniform and thus a stronger plane wave can propagate downstream. It is observed from Fig. 6 that the highest pressure point on the duct wall opposite the slanted side-branch exit moves from $x/a = 0$ to $x/a \sim 0.5$ when θ decreases from 90° to 30°. The plane wave appears to be bended toward the opposite duct wall as it leaves the side branch, probably because of the diffraction. Its energy is gradually spreading out within the junction at the same time. Very high wave pressure magnitude is localized near to the right-hand side of the side-branch exit in Fig. 6(b), suggesting that some sort of constructive interference is taking place there. This is probably due to the reflected wave from the opposite duct wall and thus a portion of the wave energy originally propagating inside the side branch is reflected back into the latter, reducing the acoustical energy downstream of the main duct. Such interference and backreflection are not observed when the slant angle θ is reduced to 30°. This explains the existence of a critical slant angle θ_c below which the sound energy can go easily into the main duct shown previously in Figs. 4 and 5. Such change of wave propagation mode should be abrupt as the mentioned interference will be much weakened at a slant angle slightly less than θ_c where most of the significant reflection from the opposite duct wall in the junction is reflected into the downstream duct. This effect also favors higher mode propagation, which will be discussed later.

A simplified schematic of the above-mentioned sound propagation mode at $\theta = \theta_c$ is summarized in Fig. 7. The arrow represents the direction of sound ray originated from the left-hand corner of the side-branch exit. The diffraction angle θ_d (angle ABC in Fig. 7) is theoretically unknown. The sound ray eventually hits the right-hand corner of the side-branch exit provided that

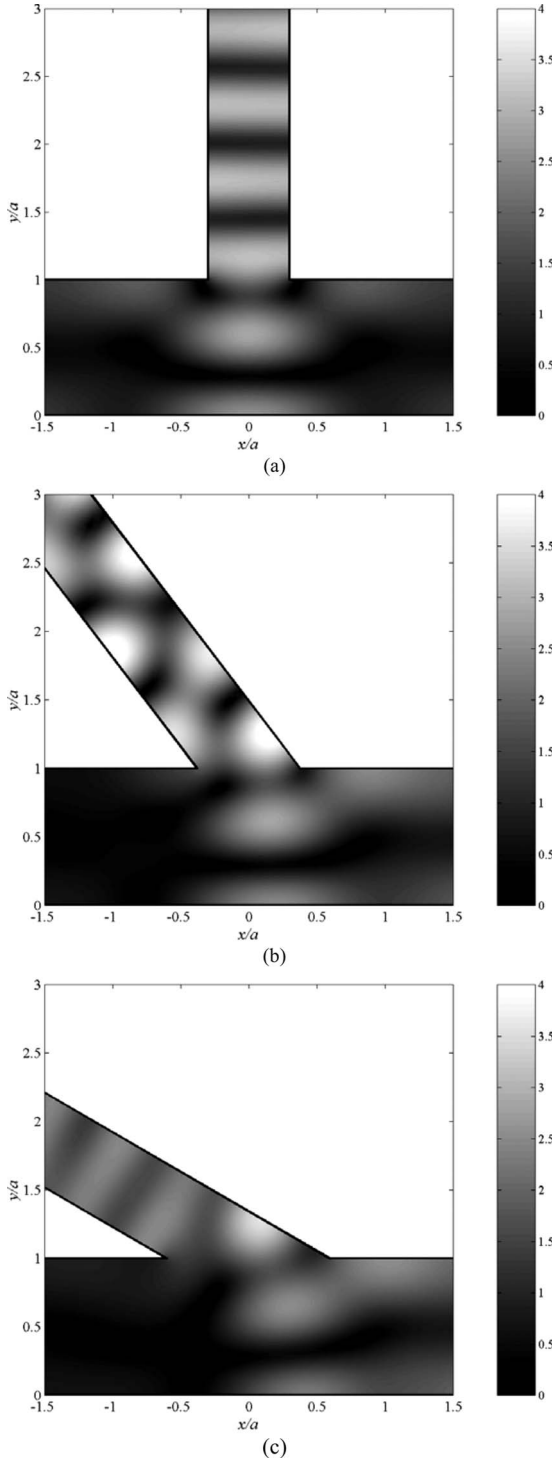

FIG. 6. Examples of sound magnitude distribution within the junction at $ka = 5.65$. (a) $\theta = 90°$; (b) $\theta = 52.5°$; and (c) $\theta = 30°$.

$$\alpha = \tan^{-1}(2a \sin \theta_c/b) = \theta_c + \theta_d. \quad (9)$$

The second part of Eq. (9) is obtained by trigonometry. Since the finite element computation suggests $\theta_c \sim 52.5°$ for $b/a = 0.6$, $\theta_d \sim 16.7°$. One can observe from Fig. 6(b) that the latter is roughly the direction beyond which the acoustical energy inside the main duct upstream of the junction center becomes insignificant. Similar θ_d is observed in Fig. 6(c) and even in Fig. 6(a). It will be shown later that both θ_d and θ_c decrease as b/a increases. The results of Figs. 4(a) and 6 also

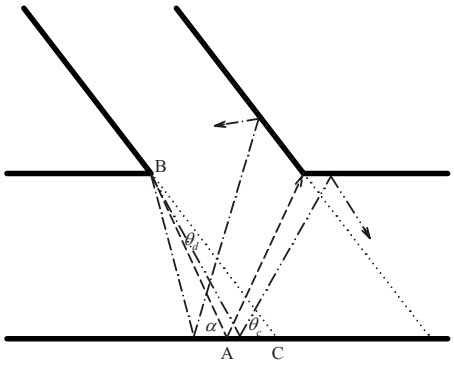

FIG. 7. Schematic for sound reflections within the junction. (---) $\theta=\theta_c$; (–·–) $\theta>\theta_c$; (–··–) $\theta<\theta_c$; (···) imaginary slanted side-branch extension.

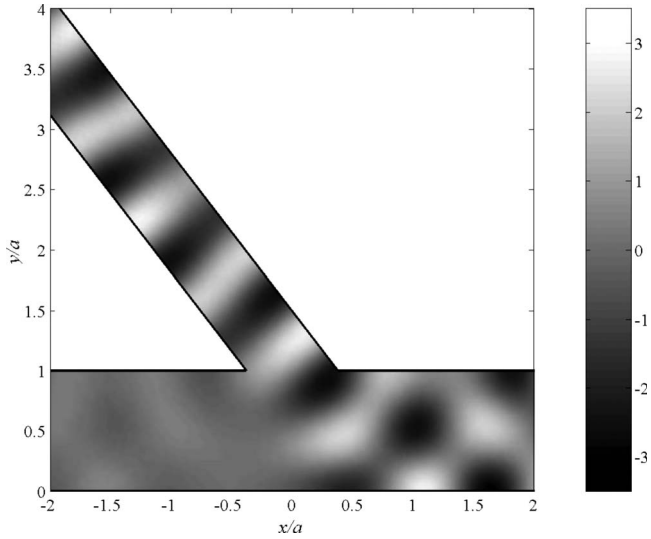

FIG. 9. Sound wave pattern within the junction for $\theta=52.5°$, $ka=8$.

tend to suggest that θ_d is not a strong function of frequency or side-branch slant angle.

For $ka>\pi$, the first asymmetric higher duct mode propagates inside the main duct. The larger the slant angle, the weaker the mode magnitude in the main duct section downstream of the junction before the cut-on of the first symmetrical higher duct mode ($m=1$) as shown in Fig. 8(a). The magnitude of the first symmetric higher duct mode ($m=2$) appears to be the highest at $\theta=\theta_c$ [Fig. 8(b)]. This is not surprising because the constructive interference that takes place at the left-hand corner of the side-branch exit tends to create an acoustic pressure pattern which matches with that of the $m=2$ duct mode at the entry of the downstream duct section. This phenomenon is illustrated in Fig. 9. The results shown in Fig. 8(b) also suggest that the $m=2$ symmetrical mode is stronger than the $m=1$ asymmetric mode for $ka>2\pi$. Besides, one can notice that the acoustic powers carried along by the higher modes concerned (proportional to $|p_d^+|^2/2$) are stronger than that associated with the plane wave.

Figure 8(c) shows the magnitude of the asymmetric mode inside the side branch. After the cut-on of the side-branch higher mode and before the cut-on of the symmetrical mode of the main duct, the mode magnitude appears to decrease with increasing θ for $\theta<\theta_c$. This trend is opposite to

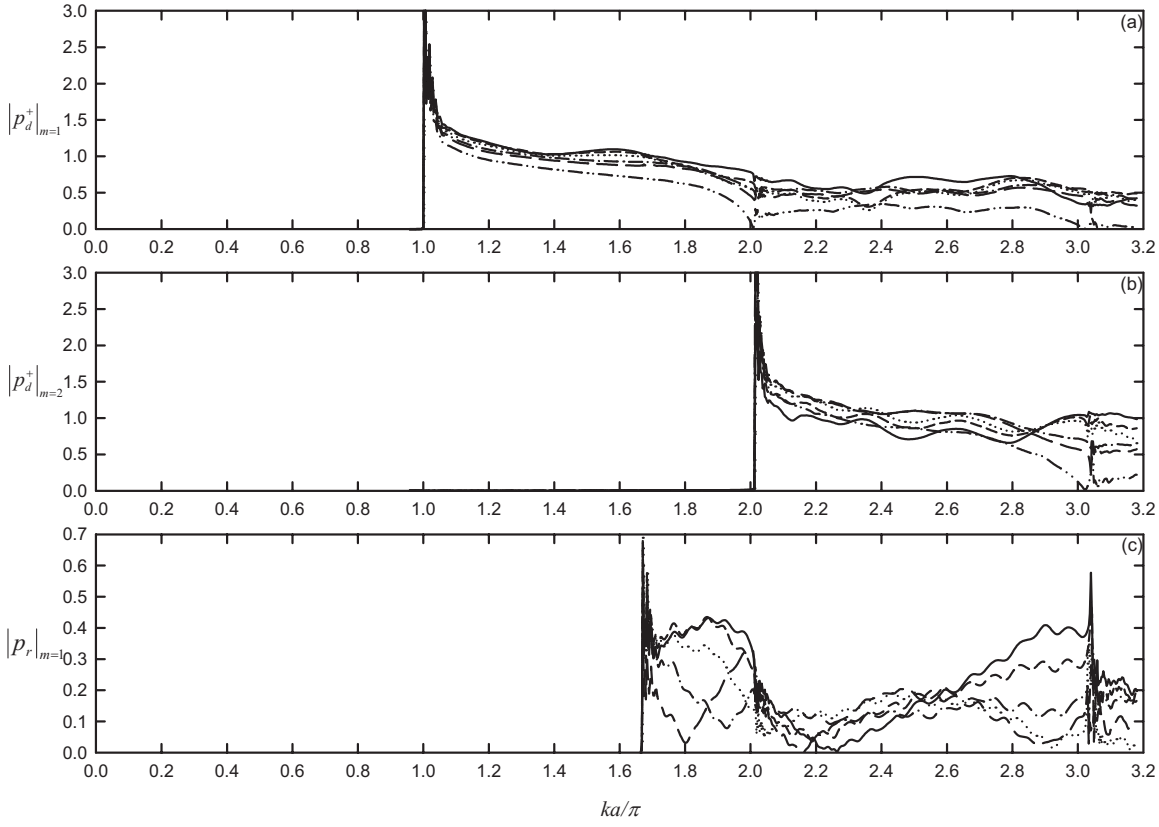

FIG. 8. Variations of higher mode magnitudes with frequency for $b/a=0.6$. (a) Downstream going $m=1$ mode in main duct; (b) downstream going $m=2$ mode in main duct; and (c) upstream going first asymmetric mode in the side branch. Legends: Same as those in Fig. 4.

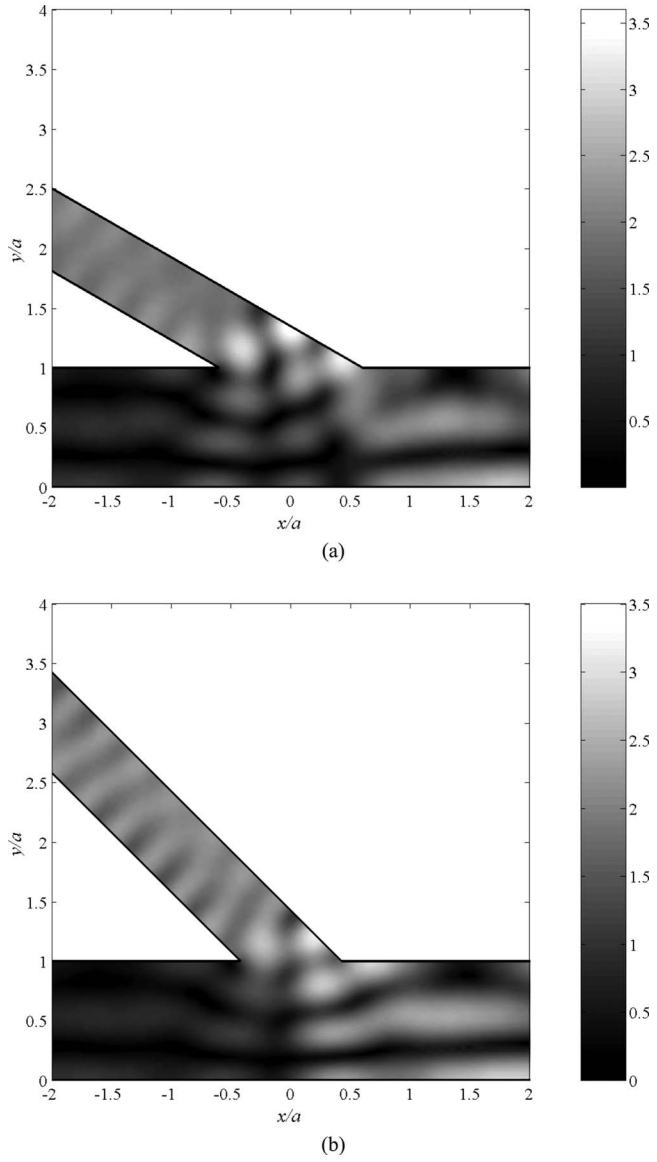

FIG. 10. Examples of sound magnitude pattern within the junction at $ka=9$. (a) $\theta=30°$ and (b) $\theta=45°$.

that of the plane wave shown in Fig. 4(c). Larger variation of the wave magnitude is found for larger slant angle. The mode magnitude rises up for $ka \to 2\pi$ near which the second asymmetric mode ($m=3$) starts to propagate along the main duct. Though the mode magnitudes at those frequencies are high for $\theta \leqslant 37.5°$, it does not increase monotonically with θ. The mode magnitude is particularly low for $\theta=45°$. Figures 10(a) and 10(b) illustrate the wave magnitude pattern within the junction for $\theta=30°$ and 45°, respectively, at $ka=9$. At higher frequencies and hence shorter wavelengths, the higher side-branch mode is well developed within the interfacing region between the side branch and the main duct at $\theta=30°$. At $\theta=45°$, the length of the interfacing region does not fit the proper development of the first asymmetric side-branch higher mode. However, one should note that such phenomenon depends on the length of the interfacing region relative to the sound wavelength and there can be a case where the higher mode is not so badly developed at $\theta>45°$.

Figure 11 illustrates the variation of the magnitude of the upstream propagating higher modes with the wave number. In general, the magnitudes of these higher modes are lower than those of the downstream going higher modes. For the asymmetric upstream going mode [Fig. 11(a)], its magnitude increases as the slant angle increases beyond 37.5°. This is rather expected as an acute θ does not favor upstream diffraction from the side-branch exit according to the well-known rectangular piston radiation characteristics.[23] The magnitude of this asymmetric mode does not depend much on the slant angle after the cut-on of the symmetrical higher mode. The magnitude of the symmetrical higher mode is also not a strong function of the slant angle. Its magnitude is also comparable to that of the asymmetric mode for $ka>2\pi$ [Fig. 11(b)].

The case of $b=a$ is a special case as the higher modes in the side branch and in the main duct will start to propagate at the same time. Figure 12 illustrates the magnitudes of the plane waves inside the system. It is again observed that there is a transition of propagation mode for the plane wave at $30° < \theta < 33°$. A more detailed investigation suggests that

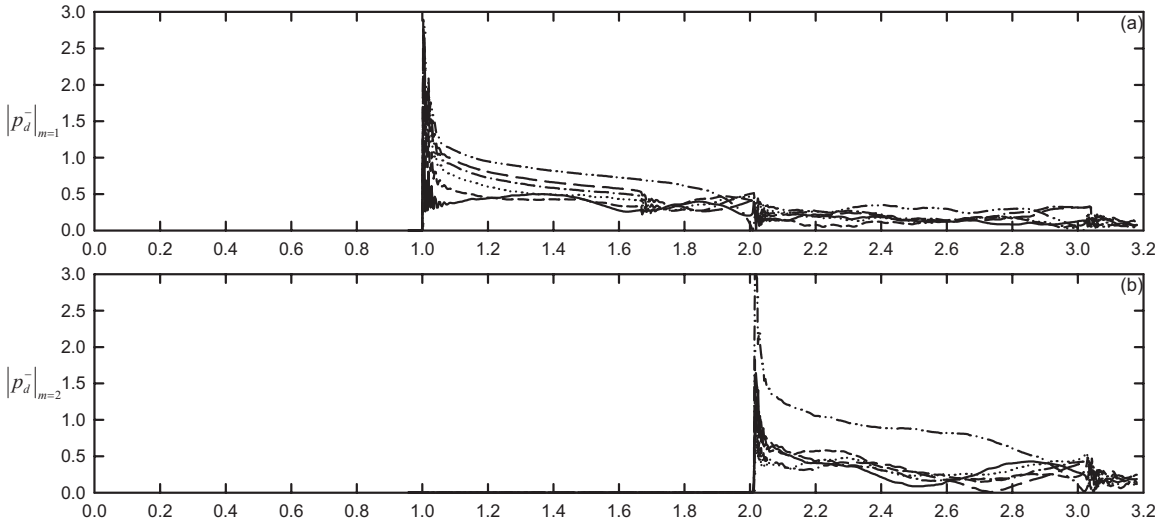

FIG. 11. Variations of upstream going higher mode magnitudes with frequency for $b/a=0.6$. (a) $m=1$ mode in main duct and (b) $m=2$ mode in main duct. Legends: Same as those in Fig. 4.

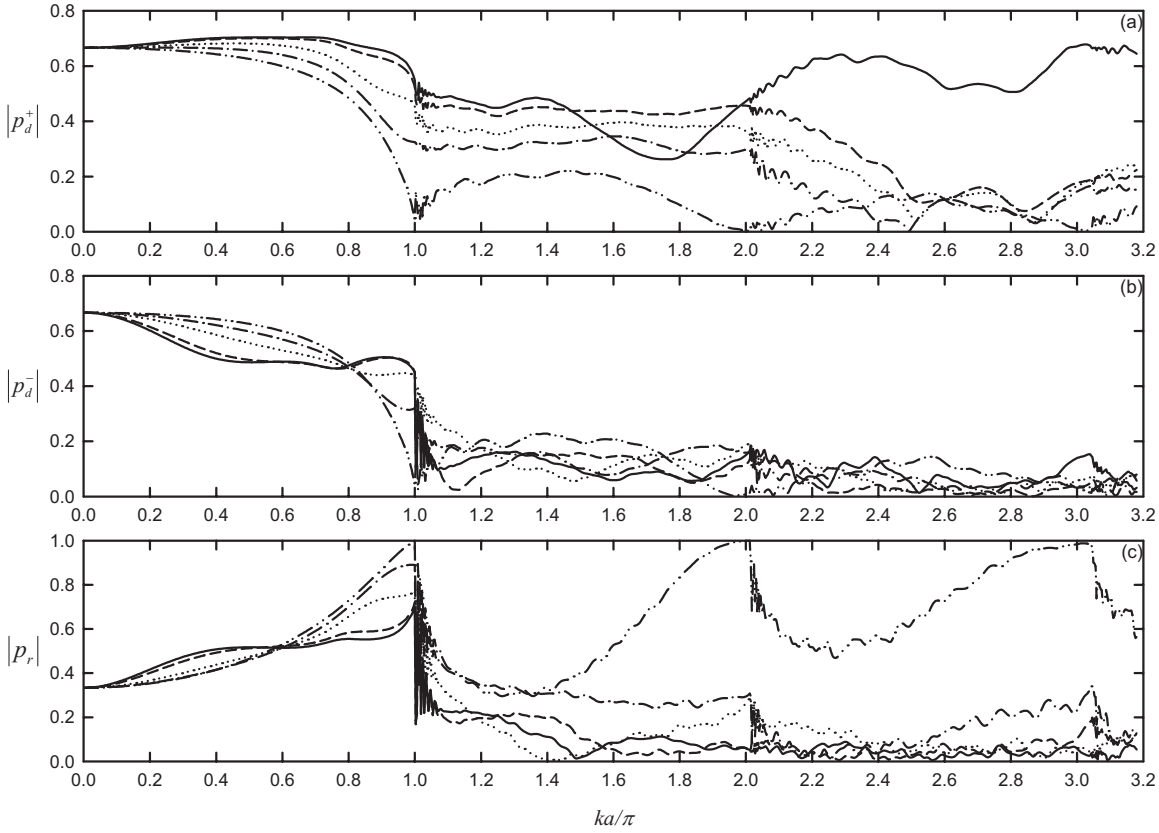

FIG. 12. Variations of plane wave magnitudes with frequency for $b/a=1$. (a) Downstream going wave in main duct; (b) upstream going wave in main duct; and (c) upstream going wave in the side branch. (—) $\theta=30°$; (---) $\theta=33°$; (···) $\theta=45°$; (–·–) $\theta=60°$; (–···–); $\theta=90°$.

the critical slant angle $\theta_c \sim 31.5°$ in this case and thus there is a slight reduction in the diffraction angle θ_d to 14.8°. For $b/a \to 0$, which is the case of a point source located on the duct wall, the diffraction angle should be large while θ_c should be small. According to Eq. (9) and the basic theory,[19,23] θ_d is capped below 90°. Figure 13 illustrates the variation of θ_d with b/a. One can observe that there is a small trough at $b/a=0.8$. The diffraction angle θ_d increases as b/a approaches 0, which is expected. However, the case for $b/a \to 0$ is not of practice interest and thus is not further discussed. It is also found that while the sudden drop of plane wave magnitude in the downstream duct due to the change in the propagation mode is significant for large b/a, those for small b/a are less pronounced (not shown here). In addition, one should note that Eq. (9) actually has two solutions for $0 < \theta_c < 90°$ when b/a is fixed. Those illustrated in Figs. 4 and 12 are the larger ones. Most of these smaller solutions are all less than 20°, which are basically of no practical significance. Nevertheless, they are presented in Fig. 13 for the sake of completeness.

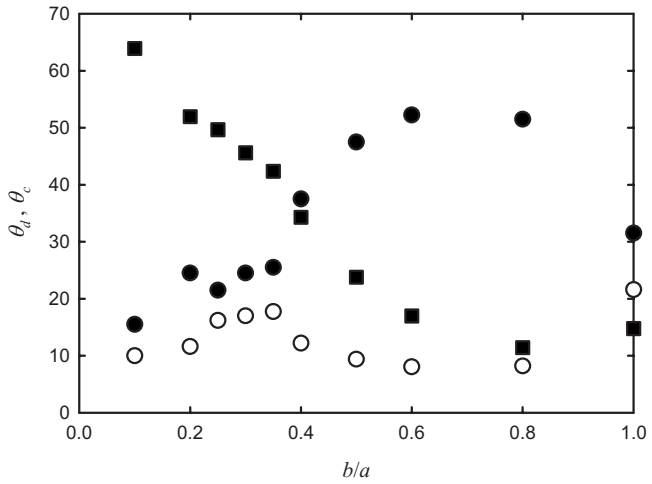

FIG. 13. Variation of θ_d and θ_c with b/a. (●) θ_c (larger solution); (○) θ_c (smaller solution); and (■) θ_d.

The behaviors of the higher mode propagation for $b/a=1$ case are very similar to those for $b/a=0.6$, except that the $m=2$ mode propagates along the slanted branch in the frequency range tested. Thus, these results are not discussed. Also, the above-mentioned wave interactions can be found at other values of b/a as far as $b < a$.

V. CONCLUSIONS

The sound propagation from a slanted rectangular side branch into an infinitely long rectangular duct of equal spanwise width and the corresponding interactions between the acoustic modes at the "side-branch-main duct" junction are investigated in the present study using the finite element method with absorptive edges at the computational domain boundaries. The relationship between the sound transmission effectiveness and the slant angle of the side branch relative to the main duct axis is examined in detail. Some theoretical deductions are also derived using the plane wave assumption. Owing to practice significance, side branches having width larger than that of the main duct are not considered.

Rectangular ducts and side branches are the most commonly found duct elements in modern buildings with centralized ventilation and air-conditioning systems.

The plane wave assumption is only valid when the forcing frequency is less than 20% of the first duct mode eigenfrequency. Before the cut-on of this duct mode frequency, the acoustical energy transmitted into the duct downstream of the junction increases with decreasing slant angle. However, the energy reflected back into the side branch decreases as the slant angle decreases. Within the frequency range studied, it is observed that the first symmetric duct mode possesses the strongest intensity, next is the first asymmetric duct mode, while the plane wave is the weakest when all these modes are coexisting.

It is also found that there exists a critical slant angle at which a drastic change in the propagation of sound will occur. A rapid drop of pressure transmission coefficient is observed when the slant angle increases beyond this critical slant angle. The angle varies with the width ratio between the side branch and the main duct. A hypothetical model incorporating a diffraction angle is set up to explain the phenomenon. It is ascribed to be due to the reflection of the diffracted sound ray at the upstream edge of the side-branch exit from the opposite duct wall, which causes significant reflection back into the side branch. The variation of this critical slant angle with the width ratio between the side branch and the main duct is determined. It is observed that this angle decreases as the width ratio decreases when the latter is less than 0.8. A slight increase of this angle is found otherwise. At or near to the critical slant angle, the magnitude and thus intensity of the first symmetric duct mode is found to be the highest.

ACKNOWLEDGMENTS

This work is supported by a grant from the Research Grant Council, the HKSAR Government (Project No. PolyU 5278/06E).

[1]L. L. Beranek, *Noise and Vibration Control Engineering, Principles and Applications* (Wiley, New York, 1992).
[2]J. W. Miles, "Diffraction of sound due to right angled joints in rectangular ducts," J. Acoust. Soc. Am. **19**, 572–579 (1947).
[3]J. C. Bruggeman, "The propagation of low-frequency sound in a two-dimensional duct system with T joints and right angle bends: Theory and experiment," J. Acoust. Soc. Am. **82**, 1045–1051 (1987).
[4]T. L. Redmore and K. A. Mulholland, "The application of mode coupling theory to the transmission of sound in the sidebranch of a rectangular duct system," J. Sound Vib. **85**, 323–331 (1982).
[5]V. Dubos, J. Kergomard, A. Khettabi, J.-P. Dalmont, D. H. Keefe, and C. J. Nederveen, "Theory of sound propagation in a duct with a branched tube using modal decomposition," Acust. Acta Acust. **85**, 153–169 (1999).
[6]S. K. Tang, "Sound transmission characteristics of Tee-junctions and the associated length corrections," J. Acoust. Soc. Am. **115**, 218–227 (2004).
[7]S. K. Tang and F. Y. C. Li, "On low frequency sound transmission loss of double side-branches: A comparison between theory and experiment," J. Acoust. Soc. Am. **113**, 3215–3225 (2003).
[8]H. G. Davies, "Noise propagation in corridors," J. Acoust. Soc. Am. **53**, 1253–1262 (1973).
[9]W. K. R. Lippert, "The measurement of sound reflection and transmission at right-angled bends in rectangular tubes," Acustica **4**, 313–319 (1954).
[10]M. Razavy, "An acoustic waveguide with variable cross section," J. Acoust. Soc. Am. **86**, 1155–1160 (1989).
[11]S. K. Lee, B. R. Mace, and M. J. Brennan, "Wave propagation, reflection and transmission in non-uniform one-dimensional waveguides," J. Sound Vib. **304**, 31–49 (2007).
[12]J. Y. Chung and D. A. Blaser, "Transfer function method of measuring in-duct acoustic properties. I. Theory," J. Acoust. Soc. Am. **68**, 907–913 (1980).
[13]S. Dequand, S. Hulshoff, H. van Kuijk, J. Willems, and A. Hirschberg, "Helmholtz-like resonator self-sustained oscillations. 2. Detailed flow measurements and numerical simulations," AIAA J. **41**, 416–423 (2003).
[14]S. K. Tang and C. K. Lau, "Sound transmission across a smooth nonuniform section in an infinitely long duct," J. Acoust. Soc. Am. **112**, 2602–2611 (2002).
[15]C. K. Lau and S. K. Tang, "Sound transmission across duct constrictions with and without tapered sections," J. Acoust. Soc. Am. **117**, 3679–3685 (2005).
[16]L. Langemyr, A. Nordmark, M. Ringh, A. Ruhe, J. Oppelstrup, and M. Dorobantu, *Partial Differential Equation Toolbox User Guide* (The MathWorks Inc., Natick, MA, 1996).
[17]L. P. George, *Automatic Mesh Generation—Application to Finite Element Methods* (Wiley, New York, 1991).
[18]N. Peake, "On the radiation properties of an asymmetric cylinder," Wave Motion **22**, 371–385 (1995).
[19]L. E. Kinsler, A. R. Frey, A. B. Coppens, and J. V. Sanders, *Fundamentals of Acoustics*, 4th ed. (Wiley, New York, 2000).
[20]L. Huang, "A theory of reactive control of low-frequency duct noise," J. Sound Vib. **238**, 575–594 (2000).
[21]M. Loéve, *Probability Theory* (Springer, New York, 1978).
[22]M. C. J. Trinder and P. A. Nelson, "Active noise control in finite length duct," J. Sound Vib. **89**, 95–105 (1983).
[23]P. M. Morse and K. U. Ingard, *Theoretical Acoustics* (McGraw-Hill, New York, 1968).